Embedded atom method potential for hydrogen on palladium surfaces

Ryan A. Ciufo^a and Graeme Henkelman^{a*}

a. Department of Chemistry and the Oden Institute for Computational Engineering and Science, University of Texas

at Austin, Austin, Texas 78712 United States.

* henkelman@utexas.edu

Abstract

The development of transferable interatomic potentials for the diffusion of hydrogen on

palladium surfaces can be of significant value for performing molecular simulations. These

molecular simulations, can, in turn lead to a better understanding of palladium-hydrogen

interactions at the atomic scale. Here, we have built upon previous work to develop an

analytical palladium-hydrogen embedded atom method (EAM) potential to better describe the

potential energy surface for hydrogen on palladium surfaces. This EAM potential reproduces

minima and transition states calculated with density functional theory for hydrogen on Pd(111)

and Pd(110) surfaces. Additionally, this potential was tested by simulating the long timescale

dynamics of hydrogen adsorbed on Pd(111). Our simulations show a barrier of ca. 0.49 eV for

hydrogen diffusion into the bulk of Pd(111), which is consistent with experimental results.

Keywords

Embedded atom method; palladium hydride; hydrogen adsorption and diffusion; adaptive

kinetic Monte Carlo

Introduction

The palladium-hydrogen system has attracted attention from applications ranging from catalysis to hydrogen purification and storage.[1-3] Palladium-hydrogen adsorption and absorption has also been studied in detail in vacuum, which has provided a fundamental understanding of the formation of palladium hydrides.[4–7] However, due to the importance of the interactions of hydrogen with palladium, either on the surface or in the bulk, there has been a desire to model these interactions to garner a better atomistic understanding. An example where such an understanding of the interaction of hydrogen with palladium, both on the surface and in the bulk, is of importance for the reductive pretreatment of palladium catalysts. These pretreatments are typically derived empirically without a detailed scientific understanding of the atomistic processes that are occurring. However, since these pretreatment methods occur over long time scales (hours to days), modern ab initio based computational methods are not capable of directly simulating the processes. To curtail this issue, empirical potentials such as the embedded atom method (EAM) can be used to reduce computational costs while increasing the accessible simulation time.[8-10] By using an empirical potential to gain atomistic insight into the evolution of catalytic surfaces, we can move towards tailoring catalytic pretreatments.

For the palladium hydride system, a number of EAM potentials have been developed to study the low (α) and high (β) hydrogen content phases. Zhou et al. developed an EAM potential based on a polynomial fit to the tabulated Pd potential data proposed by Foiles et al., which was able to predict the α and β phase miscibility gap.[11–13] Park et al. then developed a Pd-H EAM potential which also used a power series to fit the tabular Pd potential data from

Foiles et al.[14] Later, Hijazi et al. produced an analytical EAM potential for the Pd-H system, which was able to predict a number of physical properties of bulk palladium hydrides.[15] Of these analytic potentials, however, there remains an inability to accurately describe adsorbed hydrogen on palladium surfaces. The ability to model hydrogen adsorption on Pd surfaces is necessary to model the effects that hydrogen exposure has on Pd catalysts, as adsorption and surface diffusion are precursors to diffusion into the bulk.[16] Here, we build upon the work by Hijazi et al. and fit an analytic Pd-H EAM potential that can accurately describe the potential energy surface (PES) of hydrogen adsorbed on palladium surfaces.

Embedded atom method

In the embedded atom method, the total energy of the system can be written as:

$$E_{tot} = \sum_{j=1}^{N} F_i(\rho_i) + \frac{1}{2} \sum_{i=1}^{N} \sum_{\substack{j=1 \ j \neq i}}^{N} \varphi_{ij}(r_{ij})$$
 (1)

$$\rho_i = \sum_{j \neq i}^{N} f_j(r_{ij}) \tag{2}$$

where E_{tot} is the total internal energy, ρ_i is the electron density of atom i due to all other atoms, F_i is the energy to embed atom i into an electron density ρ_i , φ_{ij} is a two-body interaction potential between atoms i and j, r_{ij} is the distance between atoms i and j, and f_j is the electron density of atom j as a function of the distance from its center. To describe the Pd-Pd and H-H interactions, we have kept the analytical form proposed by Hijazi et al. where the embedding function for Pd is taken as

$$F_{Pd}(\rho) = F(\rho_e) \left[1 - \eta \ln \left(\frac{\rho}{\rho_e} \right) \right] \left(\frac{\rho}{\rho_e} \right)^n \tag{3}$$

and

$$\rho(r) = f_{\rho} e^{-\chi(r - r_{\theta})} \tag{4}$$

where f_e is a scaling constant defined by the relationship $f_e = E_c/\Omega$ where E_c is the cohesive energy and Ω is the atomic volume, r_e is the equilibrium bond length, and χ is a fitting parameter. The two-body potential for Pd-Pd and H-H are defined as

$$\varphi_{PdPd} = -\phi \left[1 + \delta \left(\frac{r}{r_e} - 1 \right) \right] e^{-\beta_{PdPd} \left(\frac{r}{r_e} - 1 \right)} \tag{5}$$

$$\varphi_{HH} = D_{HH} \left(\beta_{HH} e^{-\alpha_{HH}(r - r_{0,HH})} - \alpha_{HH} e^{\beta_{HH}(r - r_{0,HH})} \right)$$
 (6)

where ϕ , δ , β_{PdPd} , D_{HH} , β_{HH} , and α_{HH} are all adjustable parameters. The embedding energy for hydrogen is expressed using the form presented by Hijazi et al. as

$$F_{H}(\rho) = -c_{H}(\frac{1}{2+d_{H}}(\rho+\varepsilon_{H})^{2+d_{H}} - \frac{a_{H}+b_{H}}{1+d_{H}}(\rho+\varepsilon_{H})^{1+d_{H}} + \frac{a_{H}\cdot b_{H}}{d_{H}}(\rho+\varepsilon_{H})^{d_{H}})$$
(7)

and

$$\rho(r) = C_H e^{-\delta_H r} \tag{8}$$

where a_H , b_H , c_H and d_H are fitting parameters, C_H and δ_H are positive constants, and ε_H is a constant with the value 0.054. Lastly, the Pd-H pair potential is expressed using a Morse potential with the form

$$\varphi_{PdH} = D_{PdH} (1 - e^{-a_{PdH}(r_{ij} - r_{oPdH})})^2 - D_{PdH}$$
 (9)

where D_{PdH} , α_{PdH} , and r_{oPdH} are fitting parameters. Here, we keep the Pd-Pd and H-H terms proposed by Hijazi et al. (eq. 3-6, 8), and set out to fit new parameters for the Pd-H terms (eq. 7 and 9).

Fitting procedure

The parameters in equations 7 and 9 were determined by minimizing the error in energies and geometries with respect to a set of Pd-H configurations. The structures used for fitting included atomic hydrogen adsorbed to an fcc surface site on Pd(111) (H_{fcc}), hydrogen in a Pd(111) subsurface octahedral site (H_{oct}), and hydrogen in a Pd(111) subsurface tetrahedral site (H_{tetr}). In addition to these three local minima, the transition states between $H_{fcc} \rightarrow H_{oct}$, $H_{fcc} \rightarrow H_{hcp}$ on Pd(111) and the transition of hydrogen in bulk Pd from $H_{oct,b} \rightarrow H_{tetr,b}$ (as opposed to the above mentioned subsurface Hoct and Htetr sites) were used to represent higher energy structures. To capture the local curvature of the H-Pd interaction, a set of structures were included where the z coordinate of hydrogen was fixed at 0.1 Å above and below the H_{fcc} minima on Pd(111). Additionally, the energy of images to the left and right of the $H_{fcc} \rightarrow H_{hcp}$ transition state were used to capture the curvature at higher energies and reduce the chance of fitting artificial minima at the transition states. From the above structures, we were able to capture local minima, local maxima, and local curvatures in our fitting procedure. A Monte Carlo algorithm, implemented in Python, was used to minimize the error between the binding energies and geometries for the above listed minima and the relative energies for the above listed transition and intermediate states.

Computational Details

All EAM calculations were performed with the large-scale atomic/molecular massively parallel simulator (LAMMPS).[17] All density functional theory (DFT) calculations were performed using the Vienna *ab initio* simulation package. [18–21] For DFT calculations, the projector augmented wave framework was used to treat interactions between the core and valence electrons. [22, 23] Electronic exchange and correlation were described with the

generalized gradient approximation — Perdew-Burke-Ernzhof functional. [24, 25] A cutoff energy of 400 eV was used for all calculations. Methfessel-Paxton smearing was employed with a width of 0.2 eV. [26] All of the training Pd-H slabs were modelled as (4x4) unit cells with four atomic layers where the bottom two layers were frozen in bulk positions. For the PES mapping calculations, a (2x2) unit cell with five atomic layers was used where the bottom two atomic layers were frozen to bulk positions. Periodic slabs were separated by 12 Å of vacuum. The bulk Pd-H calculations were performed with a 2x2x2 unit cell with periodic boundary conditions. For the DFT calculations, the Brillouin zone was sampled with a 2x2x1, a 5x5x1 and a 11x11x11 mesh using the Monkhorst-Pack k-points scheme for the training slabs, PES mapping slabs and bulk calculations, respectively.[27] All calculations were allowed to relax until the forces on each atom were less than 0.05 eV/ Å. An optimized lattice constant of 3.89 Å was used for the EAM calculations and 3.94 Å for the DFT calculations.

The adaptive kinetic Monte Carlo (aKMC) method as implemented in the EON package was used to simulate the dynamical evolution of hydrogen on Pd(111).[28–30] The energy and force of the system were evaluated with our EAM potential. The system was modelled as a (4x4), six-layer slab with the two bottom-most layers frozen to bulk positions. The dimer method was used to explore possible reaction mechanisms and product states.[31] At each new state, dimer minimum-mode following searches were performed until a confidence value for the rate table of 0.95 was reached. The rate constant for each event was computed from the Arrhenius equation $r = A \exp\left(\frac{-\Delta E}{k_B T}\right)$, where ΔE , T and k_b are the energy barrier, temperature and the Boltzmann constant, respectively. The pre-exponential factor was calculated explicitly

from harmonic transition state theory where $A=\frac{\prod_i^{3N}v_i^{init}}{\prod_i^{3N-1}v_i^{\ddagger}}$, where v_i^{init} and v_i^{\ddagger} are the positive normal mode frequencies of the initial and saddle points, respectively. The absorbing Markov chains method was used to improve simulation efficiency by determining the escape time from superbasin states.[32]

Results

Table 1. Fitting parameters for equations 7 and 9 to describe the Pd-H interactions.

| D _{PdH} | $lpha_{PdH}$ | r oPdH | ан | b _н | Сн | dн |
|------------------|--------------|---------------|----------|----------------|----------|----------|
| 0.123452 | 5.583967 | 1.712318 | 4.245745 | 69.595833 | 0.000104 | 1.672605 |

The Pd-H pair potential and hydrogen embedding function are shown in Figure 1. The corresponding parameters for the EAM potential (equations 7 and 9) are listed in Table 1. As seen in Figure 1a, the Pd-H pair potential is narrower and exhibits weaker binding than the literature potential. Additionally, the new Pd-H pair potential has a longer equilibrium bond length of 1.71 Å as compared to the literature value of 1.30 Å. As shown in Figure 1b, there is also a significant change in the hydrogen embedding term; a more positive slope is seen as compared to what is in the literature. In the low-density region (Figure 1b, inset), the embedding term is slightly stabilizing (negative energy) below ρ = 7 and there is a significantly repulsive (positive energy) at higher densities. The decreased stabilization from the embedding term at low densities (which would be expected for adsorbed hydrogen) leads to a higher contribution to the total energy from the Pd-H pair potential. In contrast, the literature embedding term shows significant stabilization at electron densities below ρ = 17 and mild

repulsion at higher densities. This significant stabilization at densities up to ρ = 17 helps explain the significant stabilization of bulk hydride formation seen in the literature EAM potential.

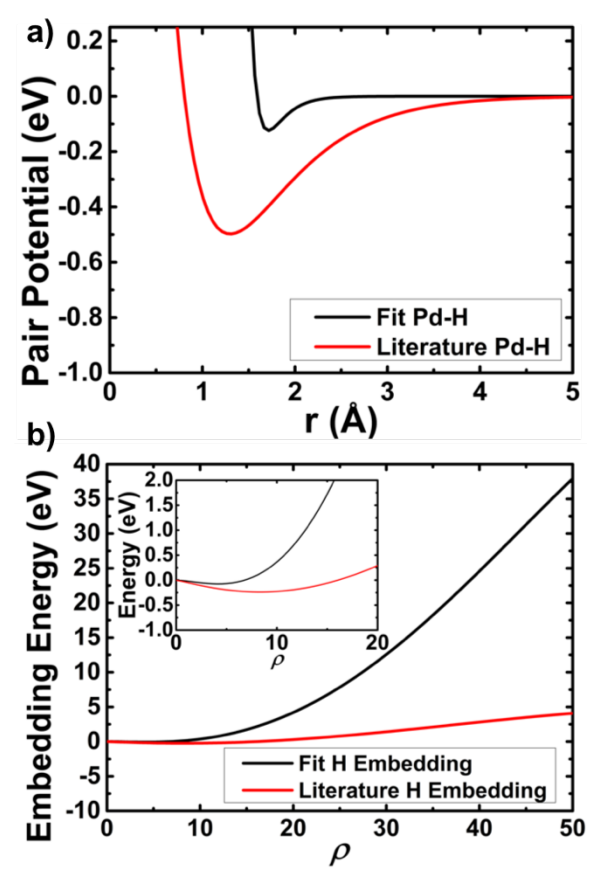


Figure 1. Our fit and literature a) Pd-H pair potential and b) hydrogen embedding term.[15]

Table 2 shows the energy and geometry results from our EAM and DFT calculations for the structures used to fit our EAM potential. It is seen that there is good agreement between the EAM and DFT binding energies, geometries and transition state barriers. The EAM potential shows slight under-binding for surface hydrogen when compared to the DFT values. In contrast, there is a slight over-binding of subsurface hydrogen for the EAM potential when compared to DFT. Finally, the EAM and DFT calculated transition state barriers align well with each other. To

ensure that our EAM potential can accurately describe regions the PES that were not included in the training set, we mapped the PES for Pd(111) using both DFT and EAM. The results, seen in Figure 2, are in good agreement with each other. For both, three-fold hollow sites are seen to be the most stable, followed by bridge and then top sites. Additionally, smooth transitions are seen between minima.

Table 2. Energies and bond lengths for hydrogen on Pd(111) and bulk Pd. Binding energies for DFT are relative to a clean Pd(111) slab and $\frac{1}{2}$ H₂. Binding energies for EAM are relative to a Pd(111) slab with hydrogen held at an infinite distance.

| | E _{Hfcc} (eV) | E _{Hoct} (eV) | E _{Htetr} (eV) | r _{Hfcc} (Å) | r _{Hoct} (Å) | r _{Htetr} (Å) | $H_{fcc} \rightarrow H_{oct}$ TS (eV) | $H_{\text{oct,b}} \rightarrow H_{\text{tetr,b}}$ TS (eV) | $H_{fcc} \rightarrow H_{hcp}$ TS (eV) |
|-----|------------------------|------------------------|----------------------------|--------------------------|--------------------------|---------------------------|---------------------------------------|--|---------------------------------------|
| DFT | 0.63 | 0.29 | 0.28 | 1.81 | 1.77/2.42 | 1.68 | 0.35 | 0.25 | 0.16 |
| EAM | 0.57 | 0.34 | 0.34 | 1.76 | 1.74/2.32 | 1.73 | 0.27 | 0.23 | 0.06 |

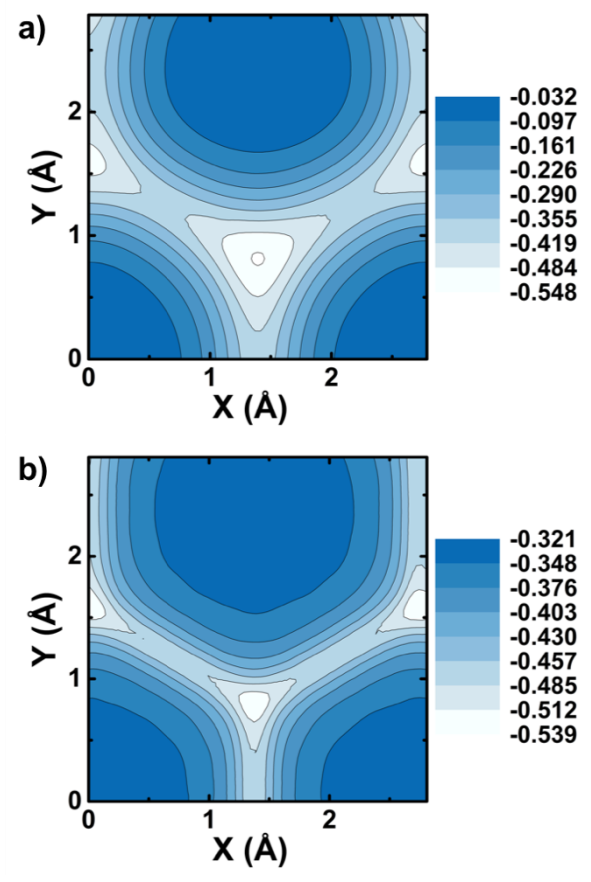


Figure 2. Potential energy surfaces for hydrogen on Pd(111) calculated using a) DFT and b) our EAM potential. The energy shown is the binding energy (eV) for hydrogen on the surface at a coverage of θ = 0.25.

To test the transferability of the EAM potential, the PES of hydrogen on the Pd(110) surface was calculated with both DFT and EAM. As seen in Figure 3, there is good agreement between the PES produced from DFT (Figure 3a) and the PES produced from EAM (Figure 3b). For the 110 surface, a slight over-binding can be observed for surface hydrogen using the EAM potential. However, it should be noted that our EAM potential can accurately describe the pseudo-hollow site as the true minima, followed by the short bridge and then the long bridge. This stands out, as EAM potentials for hydrogen on other metals, such as Cu, have been unable

to accurately reproduce the PES of the (110) surface.[33] This finding shows the transferability of our EAM potential to structures outside of our training set.

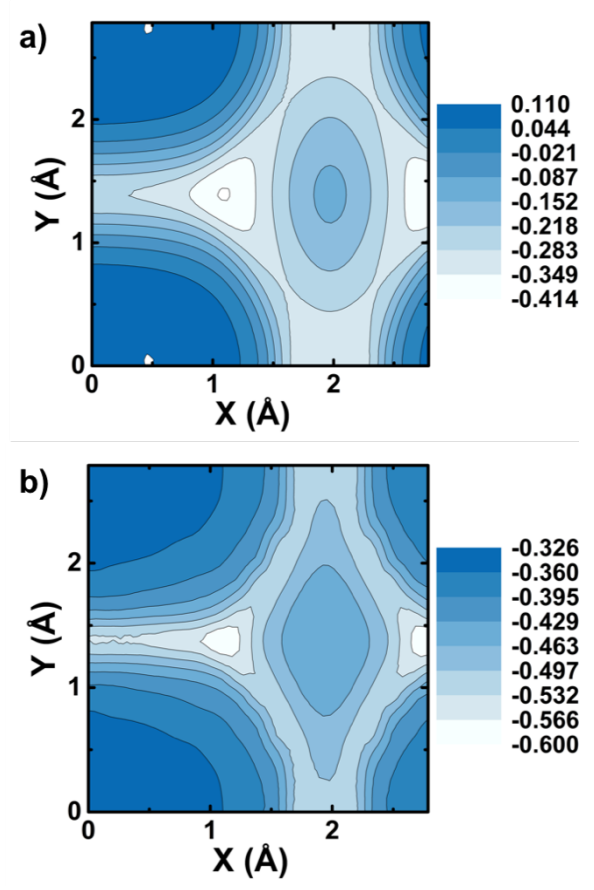


Figure 3. Potential energy surface for hydrogen on Pd(110) calculated using a) DFT and b) our EAM potential. The energy shown is the binding energy (eV) for hydrogen on the surface at a coverage of θ = 0.25.

Using our EAM potential, we performed long time scale simulations of hydrogen diffusion on Pd(111) using the adaptive kinetic Monte Carlo (aKMC) method.[28, 29] The diffusion of a single hydrogen adatom on a Pd(111) surface was modelled at 300 K. The absorbing Markov chains method was used to improve the efficiency of simulation by grouping fast transitions into superbasins via a transition counting scheme.[30,32] With this method, the surface diffusion states of hydrogen were treated as a single superbasin, where individual

transitions between the surface H states were lost, but the transition times out of the superbasin were preserved. The time evolution of the total energy of hydrogen on Pd(111) can be seen in Figure 4. Before 2.8 μ s, hydrogen is seen to diffuse across the Pd(111) surface from H_{fcc} to H_{hcp} sites by way of bridge sites. There is also diffusion from H_{fcc} to subsurface H_{oct} sites as well as from H_{hcp} to H_{tetr} sites. However, before 2.8 μ s, no transitions are seen between subsurface sites or into the second subsurface layer – all subsurface hydrogen resurfaces. After 2.8 μ s, diffusion to the subsurface was observed, where hydrogen migrates between H_{oct} sites via tetrahedral sites in the second sublayer (H_{tetr,b}). These transitions are depicted in Figure 4c.

To better represent the diffusion of hydrogen into the bulk, a disconnectivity graph was produced using the minima and transitions from the aKMC simulation (Figure 4b).[34–37] Briefly, the endpoint of each vertical line in the disconnectivity graph represent a minimum from the aKMC calculation. A vertex which connects any two minima indicates the energy of the saddle point that connects the corresponding minima. A discretization of 0.002 eV was used to distinguish between unique states. In Figure 4b, the lower black portion of the graph corresponds to hydrogen diffusion on the Pd(111) surface. The middle green portion corresponds to hydrogen in the first subsurface layer, while the upper blue portion corresponds to hydrogen diffusion into the second (bulk-like) subsurface layer. From the disconnectivity graph, we see that the energy barrier to diffuse from a surface adsorbed hydrogen to a hydrogen in the bulk is *ca*. 0.49 eV. These results are in agreement with past experimental findings that show that hydrogen penetration into the bulk of Pd foils is the rate limiting step for hydrogen absorption, with a barrier of *ca*. 0.3 - 0.4 eV.[38, 39]

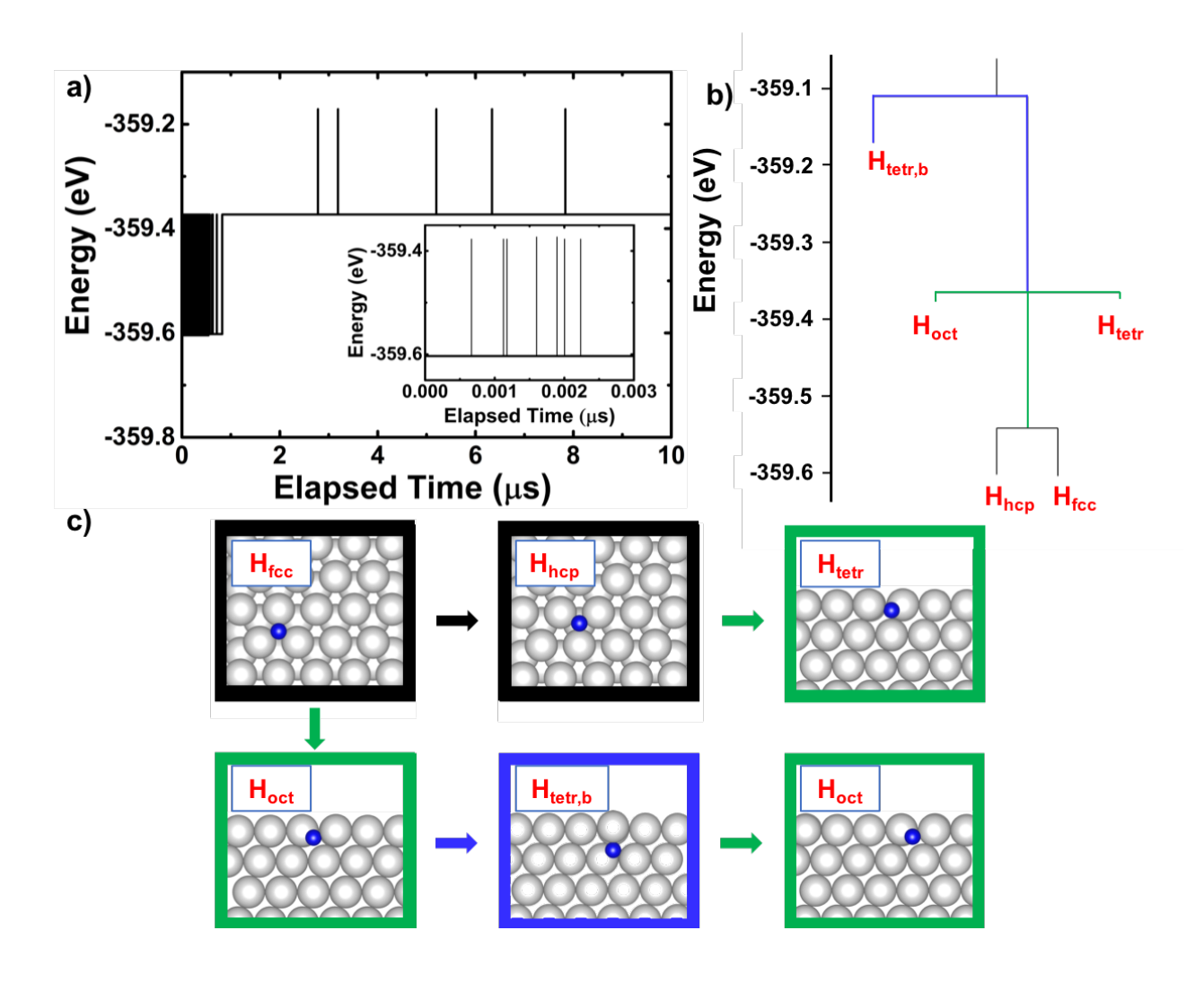


Figure 4. a) The time evolution of the total energy of hydrogen on Pd(111) at 300 K. inset) magnification of the first $0.003~\mu s$. b) A disconnectivity graph from the 5 unique states visited in the aKMC simulation. Hydrogen states in the first subsurface are colored green. Hydrogen states in the second subsurface (bulk like sites) are colored blue. c) Depictions of the states labelled in b and c where the white spheres are Pd and the blue spheres are H. The black, green and blue outlines refer to the colors from Figure 4b.

Conclusions

Using a set of three local minima, three transition states, and the local curvature around one minimum and one transition state, we were able to fit an analytic EAM potential to describe the PES of hydrogen on palladium surfaces. This EAM potential was able to accurately

reproduce the PES for hydrogen on Pd(111) and Pd(110). On Pd(110), the potential was able to capture the pseudo-hollow site as the local minima. Using the EAM potential, long time scale dynamics were performed to model hydrogen on Pd(111) at 300 K. It was seen that for the first 2.8 μ s, surface diffusion was dominant. Only after 2.8 μ s was diffusion into the bulk observed, which is consistent with past experimental findings that showed the bottleneck to hydrogen absorption is diffusion from the surface into the bulk.

Acknowledgements

This work was funded by the National Science Foundation (CHE-1764230) and the Welch Foundation (F-1841). Computational resources were provided by the Texas Advanced Computing Center and the XSEDE program.

References

- [1] Povel, R.; Feucht, K.; Gelse, W.; Withalm, G. Hydrogen Fuel for Motorcars. *Interdiscip. Sci. Rev.*, **1989**, *14* (4), 365–373.
- [2] Knapton, A. G. Palladium Alloys for Hydrogen Diffusion Membranes. *Platin. Met. Rev.*, **1977**, *21* (2), 44–50.
- [3] Adams, B. D.; Chen, A. The Role of Palladium in a Hydrogen Economy. *Mater. Today*, **2011**, *14* (6), 282–289.
- [4] Gdowski, G. E.; Felter, T. E.; Stullen, R. H. Effect of Surface Temperature on the Sorption of Hydrogen by Pd(111). *Surf. Sci.*, **1987**, *181*, 147–155.
- [5] Okuyama, H.; Siga, W.; Takagi, N.; Nishijima, M.; Aruga, T. Path and Mechanism of Hydrogen Absorption at Pd(100). *Surf. Sci.*, **1998**, *401* (3), 344–354.
- [6] Behm, R. J.; Penka, V.; Cattania, M. -G.; Christmann, K.; Ertl, G. Evidence for

- "Subsurface" Hydrogen on Pd(110): An Intermediate between Chemisorbed and Dissolved Species. *J. Chem. Phys.*, **1983**, *78* (12), 7486–7490.
- [7] Kay, B. D.; Peden, C. H. F.; Goodman, D. W. Kinetics of Hydrogen Absorption by Pd(110).

 Phys. Rev. B, 1986, 34 (2), 817–822.
- [8] Daw, M. S.; Baskes, M. I. Embedded-Atom Method: Derivation and Application to Impurities, Surfaces, and Other Defects in Metals. *Phys. Rev. B*, **1984**, *29* (12), 6443–6453.
- [9] Daw, Murray, S.; Foiles, Stephen, M.; Baskes, Michael, I. The Embedded-Atom Method:

 A Review of Theory and Applications. *Mater. Sci. Reports*, **1993**, *9* (June 1992), 251–310.
- [10] Senftle, T. P.; Janik, M. J.; Van Duin, A. C. T. A ReaxFF Investigation of Hydride Formation in Palladium Nanoclusters via Monte Carlo and Molecular Dynamics Simulations. *J. Phys. Chem. C*, **2014**, *118* (9), 4967–4981.
- [11] Zhou, X. W.; Zimmerman, J. A.; Wong, B. M.; Hoyt, J. J. An Embedded-Atom Method Interatomic Potential for Pd-H Alloys. *J. Mater. Res.*, **2008**, *23* (3), 704–718.
- [12] Foiles, S. M.; Hoyt, J. J. Computer Simulation of Bubble Growth in Metals Due to He. Sandia Rep., **2001**.
- [13] Zimmerman, J. A.; Zhou, X. W.; Griffin, J.; Wong, B. M.; Hoyt, J. J. Development of an Inter-Atomic Potential for the Pd-H Binary System. *Sandia Rep.*, **2007**.
- [14] Park, Y. H.; Hijazi, I. Development of Physics Based Analytical Interatomic Potential for Palladium-Hydride. *J. Mol. Model.*, **2017**, *23* (4), 1–11.
- [15] Hijazi, I.; Zhang, Y.; Fuller, R. A Simple Embedded Atom Potential for Pd-H Alloys. *Mol. Simul.*, **2018**, *44* (17), 1371–1379.

- [16] Lynch, J. F.; Flanagan, T. B. An Investigation of the Dynamic Equilibrium between Chemisorbed and Absorbed Hydrogen in the Palladium/Hydrogen System. *J. Phys. Chem.*, **1973**, *77* (22), 2628–2634.
- [17] Plimpton, S. Short-Range Molecular Dynamics. J. Comput. Phys., 1997, 117 (6), 1–42.
- [18] Kresse, G.; Hafner, J. Ab Initio Molecular Dynamcis for Liquid Metals. *Phys. Rev. B*, **1993**, 47 (1), 558.
- [19] Kresse, G.; J. Hafner. Liquid-Metal Amorphous-SemiconductorAb Initio Molecular-Dynamics Simulations of the Liquid-Metal-Amorphous-Semiconductor Transition in Germanium. *Phys. Rev. B*, **1994**, *49* (20), 14251.
- [20] Kresse, G.; Furthmiiller, J. Efficiency of Ab-Initio Total Energy Calculations for Metals and Semiconductors Using a Plane-Wave Basis Set. *J. / Am. Water Work. Assoc.*, **1996**, *6*, 15–50.
- [21] Kresse, G.; Furthmüller, J.; Li, Y. J.; Chen, Y. J.; Walmsley, J. C.; Mathinsen, R. H.;

 Dumoulin, S.; Roven, H. J.; Yip, S.; Supervisor, T.; et al. Efficient Iteritive Schemes for Ab

 Initio Total-Energy Calculations Using a Plane-Wave Basis Set. *Phys. Rev. B*, **1996**, *54* (16), 11169–11186.
- [22] Kresse, G.; Joubert, D. Kresse, Joubert Unknown From Ultrasoft Pseudopotentials to the Projector Augmented-Wave Method. **1999**, *59* (3), 11–19.
- [23] Blochl, P. E. Projector Augmented-Wave Method. *Phys. Rev. B*, **1994**, *50* (24), 17953–17979.
- [24] Perdew, J. P.; Burke, K.; Ernzerhof, M. Generalized Gradient Approximation Made Simple
 The PBE Functional. *Phys. Rev. Lett.*, **1996**, *77* (18), 3865–3868.

- [25] Perdew, J. P.; Burke, K.; Ernzerhof, M. Generalized Gradient Approximation Made Simple. *Phys. Rev. Lett.*, **1997**, *78*, 1396.
- [26] Methfessel, M.; Paxton, A. T. High-Precision Sampling for Brillouin-Zone Integration in Metals. *Phys. Rev. B*, **1989**, *40* (6), 3616–3621.
- [27] Monkhorst, H. J.; Pack, J. D. Special Points Fro Brillouin-Zone Integretions. *Phys. Rev. B*, **1976**, *13* (12), 5188–5192.
- [28] Xu, L.; Henkelman, G. Adaptive Kinetic Monte Carlo for First-Principles Accelerated Dynamics. *J. Chem. Phys.*, **2008**, *129* (11).
- [29] Henkelman, G.; Jónsson, H. Long Time Scale Kinetic Monte Carlo Simulations without Lattice Approximation and Predefined Event Table. *J. Chem. Phys.*, **2001**, *115* (21), 9657–9666.
- [30] Chill, S. T.; Welborn, M.; Terrell, R.; Zhang, L.; Berthet, J. C.; Pedersen, A.; Jónsson, H.;

 Henkelman, G. EON: Software for Long Time Simulations of Atomic Scale Systems. *Model.*Simul. Mater. Sci. Eng., 2014, 22 (5).
- [31] Henkelman, G.; Jónsson, H. A Dimer Method for Finding Saddle Points on High
 Dimensional Potential Surfaces Using Only First Derivatives. J. Chem. Phys., 1999, 111
 (15), 7010–7022.
- [32] Novotny, M. A. Monte Carlo Algorithms with Absorbing Markov Chains: Fast Local Algorithms for Slow Dynamics. *Phys. Rev. Lett.*, **1995**, *74* (1), 1–5.
- [33] Bae, C. S.; Freeman, D. L.; Doll, J. D.; Kresse, G.; Hafner, J. Energetics of Hydrogen Chemisorbed on Cu(110): A First Principles Calculations Study. *J. Chem. Phys.*, **2000**, *113* (16), 6926–6932.

- [34] Doye, J. P. K.; Miller, M. A.; Wales, D. J. Evolution of the Potential Energy Surface with Size for Lennard-Jones Clusters. *J. Chem. Phys.*, **1999**, *111* (18), 8417–8428.
- [35] Evans, D. A.; Wales, D. J. Free Energy Landscapes of Model Peptides and Proteins. *J. Chem. Phys.*, **2003**, *118* (8), 3891–3897.
- [36] Wales, D. J.; Miller, M. A.; Walsh, T. R. Archetypal Energy Landscapes. *Nature*, **1998**, *394* (6695), 758–760.
- [37] Becker, O. M.; Karplus, M. The Topology of Multidimensional Potential Energy Surfaces:

 Theory and Application to Peptide Structure and Kinetics. *J. Chem. Phys.*, **1997**, *106* (4),

 1495–1517.
- [38] Namba, K.; Ogura, S.; Ohno, S.; Di, W.; Kato, K.; Wilde, M.; Pletikosic, I.; Pervan, P.; Milun, M.; Fukutani, K. Acceleration of Hydrogen Absorption by Palladium through Surface Alloying with Gold. *Proc. Natl. Acad. Sci. U. S. A.*, **2018**, *115* (31), 7896–7900.
- [39] Auer, W.; Grabke, H. J. The Kinetics of Hydrogen Absorption in Palladium (α- and β-Phase) and Palladium-Silver-Alloys. *Berichte der Bunsengesellschaft für Phys. Chemie*, **1974**, *78* (1), 58–67.